Efficient Domain Decomposition Methods for Elliptic Problems Arising from Flows in Heterogeneous Porous Media

Jørg Espen Aarnes[⋆]

SINTEF Applied Mathematics, Pb. 124, Blindern, N-0314 Oslo, Norway

Abstract. In this paper we study domain decomposition methods for solving some elliptic problem arising from flows in heterogeneous porous media. Due to the multiple scale nature of the elliptic coefficients arising from the heterogeneous formations, the construction of efficient domain decomposition methods for these problems requires a coarse solver which is adaptive to the fine scale features, [4]. We propose the use of a multiscale coarse solver based on a finite volume - finite element formulation. The resulting domain decomposition methods seem to induce a convergence rate nearly independent of the aspect ratio of the extreme permeability values within the substructures. A rigorous convergence analysis based on the Schwarz framework is carried out, and we demonstrate the efficiency and robustness of the preconditioner through numerical experiments which include problems with multiple scale coefficients, as well as problems with continuous scales.

1 Introduction

Many problems of fundamental and practical importance have multiple-scale solutions. Typical examples include transport of flows in heterogeneous porous media and heat conduction in composite materials. When applying domain decomposition (DD) methods using conventional coarse grid solvers to these problems, the convergence rate may deteriorate because the coarse grid solver does not account for fine scale heterogeneous features. Hence, to attain a satisfactory convergence rate we need to use a coarse solver that reflects the small scale structures.

The Multiscale Finite Element Method (MsFEM) introduced by Hou et al. [16,17] generates a general class of coarse elliptic solvers which are adaptive to the local property of the differential operator and contain the important subgrid information. A DD preconditioner for multiscale elliptic problems using the MsFEM developed in [16,17] was proposed and analyzed in [4].

In this paper we recognize that a preconditioner of this type can serve as an efficient tool for solving elliptic problems that arise from flows in heterogeneous porous media. However, since the finite-volume method has become the standing standard in reservoir engineering communities, we incorporate the MsFEM solver into a DD algorithm for the finite volume solution of the elliptic pressure equation. The coarse subspace correction introduced here differs from the one used in [4] only in the way we construct the multiscale base functions.

To construct the coarse grid operator we need to relate the finite volume approximation space to a related finite element space. We further show how some finite volume methods are naturally related to certain mixed and non-conforming FEM's. This allows us to carry out the analysis within a variational formulation framework, and utilize the guidelines developed in [4]. The main steps in the analysis is based on the abstract Schwarz framework, [13,19,23]. To resolve the additional complexity of having multiple-scale coefficients we split the analysis into a "homogenized" part which depends on the selection of boundary conditions for the multiscale base functions, and a multiscale part which only depends on the local heterogeneous structures.

The type of elliptic problems that we encounter in reservoir simulation may have 10^6-10^{10} number of grid cells in the geological model and direct computations can easily exceed the capacity of modern computers. Moreover, in multi-phase flow simulations one solves the elliptic pressure equation for each time step, requiring a tremendous amount of computer resources. The new multiscale DD methods that we propose here can not be expected to bridge the gap between the geological scale and the reservoir simulation scale, but it might open for more accurate reservoir performance predictions by allowing simulation runs at a finer scale.

The paper is organized as follows. In section two we present the necessary mathematical background and describe the MsFEM. In section three we introduce the DD preconditioner and provide the convergence analysis. We discuss some implementational issues in section four and show some numerical results in section five. Finally we make some concluding remarks in section six.

2 Mathematical Formulations

In section 2.1 we introduce the elliptic model problem and derive the discretized equations based on a finite volume formulation. In section 2.2 we discuss the relationship between finite volume methods and some P_1 non-conforming FEM's. In section 2.3 we describe the MsFEM, [16,17], and derive the coarse grid operator. Finally, the selection of boundary conditions for the multiscale base functions is addressed in section 2.4.

2.1 Model problem and the discretized equations

We consider solving the second-order elliptic equation

$$-\nabla \cdot (a(x)\nabla u) = f \qquad \text{in } \Omega \subset \mathcal{R}^d , \qquad (1)$$
$$u = 0 \quad \text{on } \partial\Omega , \qquad (2)$$

where $a(x) = (a_{ij}(x))$ a symmetric and positive definite tensor with uniform upper and lower bounds:

$$0 < \alpha < \frac{\xi \cdot a(x)\xi}{\xi \cdot \xi} < \beta < \infty, \quad \forall \xi \in \mathcal{R}^d\backslash\{0\}, \ \forall x \in \Omega.$$

Eqn. (1) may represent single-phase porous media flow or steady state heat conduction through a composite material. These are typical examples of problems where $a(x)$ can span over many length scales and the solution of (1)-(2) displays a multiple-scale structure.

We discretize the domain Ω on two scales with mesh parameters h and H, $h \ll H$. Thus, let $\mathcal{T}^h$ and $\mathcal{K}^H$ be partitionings of Ω into polygons or polyhedrons with typical diameters h and H respectively. We do not require that $\mathcal{T}^h$ forms a sub-partitioning of each $K \in \mathcal{K}^H$, but, for simplicity, we assume that $a(T)$ is a constant (symmetric positive definite) tensor for each $T \in \mathcal{T}^h$. We associate with $\mathcal{T}^h$ the space of piecewise constants,

$$V^h = \{v \in L^2(\Omega) : v|_T = constant , \ \forall T \in \mathcal{T}^h\} ,$$

and denote by N^h the dimension of V^h. Observe that, by assumption, we have $a(x) \in (V^h)^{d \times d}$.

For the fine mesh discretization we apply the popular cell centered finite volume method, see e.g. [1,2,15]. To derive the discrete equations it is convenient to introduce a new variable $q = -a(x)\nabla u$ so that the left hand side of (1) becomes $\nabla \cdot q$. We remark that q is the Darcy velocity in porous media flow and the thermal flux density for heat transfer in composite materials. The finite volume method is based on the conservation law,

$$\int_{\partial T} q \cdot n \, dS = \int_T f \, dV , \qquad \forall T \in \mathcal{T}^h . \qquad (3)$$

Note that if q is sufficiently smooth, then

$$\int_T \nabla \cdot q \, dV = \int_{\partial T} q \cdot n \, dS ,$$

by virtue of the Gauss-Green theorem. We observe that eqn. (3) ensures mass conservation within each of the control volumes $T \in \mathcal{T}^h$. In the finite volume method we rewrite (3) in discrete form by approximating the net flux out of each cell on the basis of the potentials (or pressures) in a certain number of neighboring cells. The general finite volume formulation is thus on the form

$$\sum_{j,k} t_{ij}^k g_{ij}^k(v^h) = \int_{T_i} f \, dx , \qquad i = 1, \dots, N^h , \qquad (4)$$

where the g_{ij}^k's are pressure dependencies for the interface $S_{ij} = \partial T_i \cap \partial T_j$ and the t_{ij}^k's are corresponding transmissibilities. For brevity we write (4) as

$$\Sigma^h v^h = F^h . \qquad (5)$$

First assume that $\mathcal{T}^h$ is a partitioning of Ω into parallelepipeds and denote by n_{ij} the unit normal to S_{ij} pointing from T_i to T_j. $\mathcal{T}^h$ is said to be a-orthogonal if

$$n_{ij} \cdot a(T_i)n_{ik} = 0 , \qquad j \neq k , \ \forall T_i \in \mathcal{T}^h .$$

The notion of a-orthogonality generates a class of problems for which one may discretize (3) using a two-point flux approximation scheme

$$\sum_j t_{ij}(v_i - v_j) = \int_{T_i} f \, dx , \qquad i = 1, \dots, N^h , \qquad (6)$$

where the transmissibilities are defined by,

$$t_{ij} = \frac{A_{ij}}{d_i k_i^{-1} + d_j k_j^{-1}} . \qquad (7)$$

Here d_i and d_j are the respective distances from the cell centers to the interface S_{ij} along the line segment connecting the cell centers. Furthermore, A_{ij} is the surface area of S_{ij} and $k_l = n_{ij} \cdot a(T_l)n_{ij}$, $l = i, j$.

While two-point flux approximation schemes may be natural and sufficient for problems on a-orthogonal grids, they may be equally insufficient for non a-orthogonal grids, [3,14]. For general polygonal or polyhedral grids we need to allow multi-point flux approximations to obtain better predictions of the velocity field. We shall see below that the two-point flux approximation (6) on a-orthogonal quadrilateral grids in 2D is equivalent with the standard non-conforming P_1 FEM on a dual sub-triangulation of $\mathcal{T}^h$. Similarly, we describe how the P_1 non-conforming FEM on a different type of dual grid is naturally related to certain multi-point flux approximation schemes. The primary benefit of working with the finite volume method rather than the P_1 non-conforming FEM is that we have fewer unknowns in the discretized equations and that the grid structure is generally simpler, in particular in 3D.

2.2 Relationship to finite element methods

It has been known for some time that the linear systems arising from (1)-(2) using certain mixed and non-conforming FEM's are equivalent, [5,10]. The purpose of the following is to argue that the finite volume methods are naturally related to these methods, and in some cases equivalent. To keep the presentation simple we only work with the P_1 non-conforming FEM. More general non-conforming FEM's, and their relation to the finite volume methods (4), are treated similarly.

The standard P_1 non-conforming FEM is equivalent with the lowest order Raviart-Thomas mixed FEM, [5]. This equivalence implies that there is an isomorphism between the approximation space U^h for the P_1 non-conforming FEM and the approximation space $Q^h \subset H^1_{div}(\Omega)$ for the flow variable q in the equivalent Raviart-Thomas mixed FEM. Hence, if we can prove an equivalence between a finite volume method (4) and the P_1 non-conforming FEM, then there is also a mapping from V^h onto Q^h. This mapping will be uniquely determined by the fluxes across the cell interfaces S_{ij} and will allow us to view the finite volume solution $v^h \in V^h$ as a member of $H^1_{div}(\Omega)$.

Let $\mathcal{X}^h$ be a triangulation of Ω and define the standard non-conforming P_1 finite element space $U^h(\mathcal{X}^h)$,

$$U^h(\mathcal{X}^h) = \{u \in L^2(\Omega) : u|_X \in P_1(X), \; \forall X \in \mathcal{X}^h,$$

u is continuous at the midpoints of interior sides

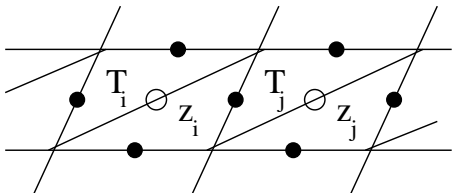and vanish at the midpoints of sides on $\partial\Omega\}$,

and supply $U^h(\mathcal{X}^h)$ with the usual bilinear form,

$$a^h(u,v) = \sum_{X \in \mathcal{X}^h} \int_X \nabla u \cdot a(x) \nabla v . \qquad (8)$$

The non-conforming P_1 finite element solution u^h to (1)-(2) is now defined by,

$$a^h(u^h, v) = (f, v) , \qquad \forall v \in U^h , \qquad (9)$$

where $(\cdot, \cdot)$ denotes the standard L^2 inner product on Ω.

Fig. 1. A quadrilateral parallelepiped mesh $\mathcal{T}^h$ and its dual triangulation $\mathcal{X}^h$. The black dots denote the Y^h nodes and the hollow circles denote the Z^h nodes.

First assume that $\mathcal{T}^h$ is an a-orthogonal grid in 2D, and let $\mathcal{X}^h$ be the triangulation of Ω formed by subdividing each parallelepiped into two conformal triangles, see Figure 1. Denote by Z^h the set of nodes on the diagonals, i.e. cell centers, and by Y^h the set of nodes on the midpoints of the parallelepiped edges. Now, define the nodal map $L^h : V^h \to U^h$ by

$$a^h(L^h v, u) = 0 , \qquad \forall u \in U^h , \; u = 0 \text{ on } Z^h . \qquad (10)$$

Hence, if $u = L^h v$, $v \in V^h$ and $y_{ij} \in S_{ij} \cap Y^h$ then

$$\frac{u(z_i) - u(y_{ij})}{|y_{ij} - z_i|^2}(y_{ij} - z_i) \cdot a(T_i) n_{ij} =$$

$$\frac{u(y_{ij}) - u(z_j)}{|y_{ij} - z_j|^2}(z_j - y_{ij}) \cdot a(T_j) n_{ij} .$$

This relation states $q \cdot n_{ij}$ is continuous at y_{ij}, and hence, by linearity, across S_{ij}.

To see that the two-point flux approximation scheme (6) on the a-orthogonal grid $\mathcal{T}^h$ and the non-conforming FEM (9) on the dual subgrid $\mathcal{X}^h$ give rise to equivalent linear systems under the correspondence induced by L^h, we only need to show that the linear system (5) with the transmissibilities (7) is obtained by eliminating the variables associated with the vertex nodes Y^h from the P_1 finite element stiffness matrix. To this end, observe that the a-orthogonality implies that the Y^h nodes are not mutually connected, and can hence be eliminated using simple local algebraic manipulations. It is straight forward to check that this elimination process results in the harmonic averaged coupling induced by (7). This implies that $u^h = L^h v^h$ and, in particular, that the flux across S_{ij} generated by v in (6) coincides with the flux generated by $L^h v$ in the physical space U^h. Thus, if $(\cdot, \cdot)_\Sigma = (\Sigma^h(\cdot), \cdot)$ then the norm identity

$$(v, v)_\Sigma = a^h(L^h v, L^h v) , \qquad \forall v \in V^h . \qquad (11)$$

holds for all $v \in V^h$.

For general quadrilateral grids in 2D one can not remove the extra variables induced by the dual triangulation using only local algebraic manipulations. This reflects that the two-point flux-approximation is no longer appropriate, and is in fact not convergent in general [3, 14]. However, this ability to eliminate variables on the cell boundaries using local algebraic manipulations is a cornerstone in the construction of multi-point flux approximation (MPFA) schemes. MPFA schemes are often derived by constructing local interaction regions and supplying them with a finite element-like space. The transmissibilities and pressure dependencies are then obtained by eliminating the variables on the interfaces. We shall consider the popular O-method, [1,2], in detail and show that it is, by construction, the linear system we obtain by eliminating variables on the cell boundaries from a special, non-standard, non-conforming P_1 FEM. We consider only quadrilateral grids in 2D, but the same reasoning applies to more general polygonal grids in 2D and polyhedral grids in 3D.
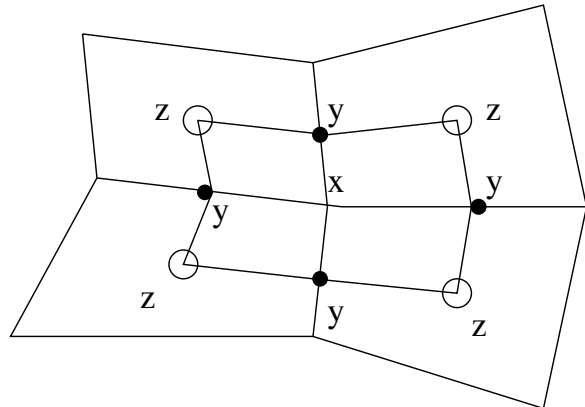
Fig. 2. A quadrilateral mesh $\mathcal{T}^h$ and its MPFA dual grid $\mathcal{X}^h$. The black dots denote the Y^h nodes and the hollow circles denote the Z^h nodes.

Hence, let $\mathcal{T}^h$ be a quadrilateral grid in 2D and let $\mathcal{X}^h$ be the quadrilateral dual grid obtained by subdividing each quadrilateral into four sub-quadrilaterals with vertices at the cell centers, Z^h, the midpoints of the cell edges, Y^h, and the cell vertices, X^h, see Figure 2. For each $x_i \in X^h \cap \Omega$ we associate the interaction region $R(x_i) = \cup\{X \in \mathcal{X}^h : \partial X \cap x_i \neq \emptyset\}$. We then define the following non-conforming P_1 finite element space

$$U^h(\mathcal{X}^h) = \{u \in L^2(\Omega) : u|_X \in P_1(X), \ \forall X \in \mathcal{X}^h,$$

u is continuous at Z^h, semi-continuous at $Y^h \cap \Omega$

$$\text{and vanish on } Y^h \cap \partial\Omega\} .$$

By semi-continuous at $y \in Y^h \cap \partial R(x)$, $x \in X^h$, we mean that it has a continuous limit at y as a function defined on $R(x)$. A function $u \in U^h(\mathcal{X}^h)$ is therefore in general discontinuous at Y^h. Formally, this means that in the discrete finite element equations we have two nodes representing each grid point in Y^h. This implies that the Y^h nodes only depend on each other within each interaction region, and they can therefore be removed from the non-conforming finite element equations with local algebraic manipulations. The O-method is defined to be the linear system of equations we obtain after this elimination process. We thus see that the map (10) again induces the proper norm identity (11) on V^h.

For some MPFA schemes it may be difficult to define an appropriate non-conforming finite element space U^h on a dual grid and a corresponding map $L^h : V^h \to U^h$ so that the norm identity (11) holds. However, for the convergence analysis it is sufficient to have an equivalence relation,

$$(v,v)_\Sigma \lesssim a^h(L^h v, L^h v) \lesssim (v,v)_\Sigma , \qquad \forall v \in V^h . \quad (12)$$

Here $A(x) \lesssim B(x)$ means that there exist a positive constant c independent of the mesh-parameters and the problem coefficients so that $A(x) \leq cB(x)$ for all $x \in \Omega$. The preceding discussion should provide some helpful guidelines for how one can construct MPFA schemes that may satisfy (12).

2.3 Multiscale finite element methods

In order to capture the effect of the small scale details on the large scales without resolving the small scale features, Babuška and Osborn [7] (for one dimensional problems), Babuška, Caloz and Osborn [6] (for special 2D problems) proposed the generalized FEM's by introducing special base functions based on the differential operator. Hou and Wu, [16], and Hou, Wu and Cai, [17], generalized the idea in [7] to two dimensions and proposed a multiscale finite element basis by solving local leading order homogenization problems. The basic convergence property was established for two scale periodic coefficients in 2D [17]. It was shown that the solution converges to the homogenized solution in the homogenization limit $\epsilon \to 0$.

Chen and Hou [11] recently developed a mixed multiscale FEM motivated by the numerical simulation of flow transport in heterogeneous porous media. Both methods [11,16] can be reformulated within a finite volume framework by constructing the base functions as local finite volume solutions with prescribed boundary conditions. We shall briefly outline the MsFEM [16] and show how to reformulate it in a finite volume framework. The mixed MsFEM [11] can be reformulated along the same lines, but for reasons concerning the convergence analysis, and because the mixed variant does not seem to give any major benefits in the DD iteration, we restrict our attention to the MsFEM in its original form.

Define the usual bilinear form on $H_0^1(\Omega)$,

$$a(u,v) = \int_\Omega \nabla u(x) \cdot a(x) \nabla v(x) \, dx .$$

The variational formulation of (1)-(2) is then to seek $u \in H_0^1(\Omega)$ such that,

$$a(u,v) = (f,v) , \qquad \forall v \in H_0^1(\Omega) . \quad (13)$$

The base functions $\psi_K^i \in H^1(K)$ for the MsFEM introduced in [16] satisfy the homogeneous equation,

$$a(\psi_K^i, v) = 0 , \qquad v \in H_0^1(K) , \ i = 1, \dots, n(K) , \quad (14)$$

where $n(K)$ is the number of base functions with support in K. To make (14) well posed we need to specify boundary conditions on ∂K, but for now we just assume that

$$V_0 = span\{\psi_K^i : K \in \mathcal{K}^H, \ i = 1, \dots, n(K)\} \subset H_0^1(\Omega) .$$

The MsFEM solution $u_0 \in V_0$ is defined by

$$a(u_0, v) = (f, v) , \qquad \forall v \in V_0 . \quad (15)$$

For brevity we write this equation in operator form: $A_0 u = u_0$, where we refer to A_0 as the continuous (as opposed to discrete) multiscale finite element operator.

We turn to the finite volume formulation of (14). The idea is to use the finite volume method to construct the multiscale bases and interpret the base functions as functions in a finite element dual space. We now assume that $\mathcal{T}^h$ also forms a sub-partitioning of each $K \in \mathcal{K}^H$. We let U^h be a dual non-conforming finite element space supplied with the non-conforming bilinear form (8) and assume that $L^h : V^h \to U^h$ is a linear map so that the equivalence relation (12) holds true. For each K we denote by Σ_K the local stiffness matrix in K and define the multiscale finite volume base functions v_K^n, $K \in \mathcal{K}$, $n = 1, \dots, n(K)$, to be the solution to the homogeneous equation,

$$\Sigma_K v_K^n = 0 \quad \text{in } K , \quad (16)$$
$$v_K^n = \mu_K^n \quad \text{on } \partial K , \quad (17)$$

where μ_K^n is some prescribed boundary data on ∂K. Now, let $\phi_K^n = (L^h v_K^n)|_K$, $V_0^h = span\{v_K^n\}$, $U_0^h = L^h V_0^h$ and define the multiscale finite volume - finite element solution $v_0^h = (L^h)^T u_0^h$ where $u_0^h \in U_0^h$ is defined by

$$a^h(u_0^h, v) = (f, v) , \ \forall v \in U_0^h . \quad (18)$$

We also write this equation in operator form: $A_0^h u^h = u_0^h$ where $u^h = L^h v^h$. Hence, it follows that $v_0^h = T_0 v^h$ where $T_0 = (L^h)^T A_0^h L^h$ is the discrete (finite volume) MsFEM operator.

2.4 Boundary conditions for the base functions

In one dimension the boundary conditions for the multiscale base functions are determined by $\mu^i(x_j) = \delta_{ij}$, $x_j \in \Gamma := \partial \mathcal{K}^H \backslash \partial \Omega$. We demonstrate that this leads to the special super convergence result $u_0 = u_I$ where u_I is the interpolant of u in V_0, i.e. the unique function in V_0 with $u_I = u$ on Γ. Indeed, since $u - u_I$ vanishes on Γ, we have

$$a(u_I, v) = a(u, v) = (f, v) , \quad \forall\, v \in V_0 .$$

Thus, by (15) and choosing $v = u_I - u_0$ we obtain

$$a(u_I - u_0, u_I - u_0) = 0 ,$$

which implies $u_0 = u_I$. The solution to (13) can thus be decomposed as $u_0 + u_*$ where u_* is defined by,

$$a(u_*, v) = (f, v) , \quad \forall v \in H_0^1(\mathcal{K}^H) .$$

Hence, we see that the variational problem (13) in one dimension is naturally decomposed into a coarse subspace correction in V_0 and independent local solves.

There is, however, a fundamental difference between 1D and higher dimensional problems since the "resonance error" caused by non-matching boundary conditions only occurs in multi-D. Therefore the selection of proper boundary conditions for the base functions become important to achieve accurate approximations. It was e.g. observed in [16,17] that $u - u_0$ may display a boundary layer structure within the coarse grid elements if improper boundary conditions are chosen. In fact, since the multiscale base functions satisfy the homogeneous equation (14) or (16), the boundary conditions determines how well the local property of the operator is sampled into the base functions.

To clarify the relation between the approximation properties of A_0 and the selected boundary conditions for the multiscale base functions, let $\Gamma = \partial \mathcal{K}^H \backslash \partial \Omega$ and define

$$M = \{ \mu = v|_\Gamma : v \in H_0^1(\Omega) \}$$

and

$$M_0 = \{ \mu = v|_\Gamma : v \in V_0(\Omega) \} .$$

Thus, M_0 is the space spanned by the boundary conditions for the multiscale base functions.

Now, define the space W_a consisting of generalized harmonic functions

$$W_a = \{ w \in H_0^1(\Omega) : a(w, v) = 0 , \ \forall v \in H_0^1(\mathcal{K}^H) \} ,$$

and the associated extension operator $H_a : M \to W_a$,

$$a(H_a \mu, v) = 0 , \ \forall v \in H_0^1(\mathcal{K}^H) .$$

We can then reformulate (13) as follows: Find $\mu \in M$ and $u_* \in H_0^1(\mathcal{K}^H)$ such that,

$$a(H_a \mu, H_a \nu) = (f, H_a \nu) , \quad \forall \nu \in M , \tag{19}$$

$$a(u_*, v) = (f, v) , \quad \forall v \in H_0^1(\mathcal{K}^H) . \tag{20}$$

We then recover u in (13) with the generalized harmonic extension $u = H_a \mu + u_*$.

The relevant bilinear form for the alternative formulation (19) is $(\mu, \nu)_M = a(H_a \mu, H_a \nu)$. Now, since

$V_0 \subset W_a$ and u_0 is the orthogonal projection of u onto V_0 with respect to $a(\cdot, \cdot)^{1/2}$, it follows that $\mu_0 = u_0|_\Gamma$ is the orthogonal projection of μ onto M_0 with respect to $(\cdot, \cdot)_M^{1/2}$. This implies that A_0 is optimal, in a certain sense, for non-overlapping DD algorithms among all coarse solvers $A^H : H_0^1(\Omega) \to V^H$ with $V^H|_\Gamma = M_0$.

Computational experience indicate that the use of boundary conditions which adapt to the heterogeneous structures on the element boundaries in general lead to better accuracy than simple (smooth) boundary conditions. But they do not necessarily achieve faster convergence of the DD iteration consisting of additional local solves. To understand this we should keep in mind that the coarse solver usually act the role of removing low frequency errors, while the local solves remove high frequency errors. In particular, we shall see that for the proposed multiscale DD methods the boundary conditions for the multiscale base functions determine how well we capture the "homogenized" part of the solution.

The role of the boundary conditions for the base functions is thus to generate a good coarse space M_0 in M. We wish to point out that allowing non-matching boundary conditions so that $V_0 \not\subset H_0^1(\Omega)$ can improve the convergence rate for the DD iteration in the same way the non-conforming FEM's may give superior performance to the analogous conforming FEM's. For instance, it is well known that if the subdomains have sufficient overlap, then the non-conforming linear FEM coarse solver allows an optimal rate of convergence for the preconditioning of elliptic problems with quasi-homogeneous coefficients, [22]. On the other hand, we know that the conforming linear FEM coarse solver induce a suboptimal rate of convergence, [8].

3 The Domain Decomposition Preconditioner

Many non-overlapping DD methods can be categorized as so-called Schwarz methods for which a simple framework for the convergence analysis exists, [13,19,23,24]. The abstract Schwarz framework is based on a splitting of a finite dimensional Hilbert space V into subspaces with in general much smaller dimension. Thus, let V_i be a sequence of finite dimensional Hilbert spaces and let $I_i : V_i \to V$ be a corresponding sequence of interpolation-like operators such that V allows the following decomposition,

$$V = \sum_{i=0}^{p} I_i V_i := \left\{ v : v = \sum_i I_i v_i, \ v_i \in V_i \right\} .$$

The space V_0 represents a coarse global approximation space while V_i, $1 \le i \le p$, are subspaces corresponding to some localized region in space. Let V be supplied with a symmetric positive definite bilinear form $a(\cdot, \cdot)$ and assume that each V_i is supplied with an auxiliary symmetric positive definite bilinear form $(\cdot, \cdot)_i$ on V_i which approximates $a(\cdot, \cdot)$ on V_i in the following sense:

$$a(I_i v, I_i v) \le \omega(v, v)_i , \ \forall v \in V_i , \ \forall i .$$

The parameter ω is assumed to be bounded and plays a special role in the analysis of Schwarz methods. Now, define the projection-like operators $T_i : V \to V_i$ by,

$$(T_i u, v)_i = a(u, I_i v) , \ \forall u \in V, \ \forall v \in V_i .$$

Finally, let $\mathcal{P}$ be a polynomial with no zero order term and suppose we want to find $u^* \in V$ such that

$$a(u^*, v) = f(v) , \quad \forall v \in V , \ f \in V' . \tag{21}$$

The idea behind the abstract Schwarz method is to replace (21) with a better conditioned operator equation

$$\mathcal{P}(T_0, \ldots, T_p) u = g^* ,$$

where $g^* = \mathcal{P}(\{T_i\}) u^*$. The additive Schwarz method is e.g. obtained by choosing $\mathcal{P}(\cdot) = \sum_{i=0}^{p} T_i$. The following result bounds the condition number for the preconditioned abstract additive Schwarz method [19,23].

Theorem 1 *Let C_0 be a positive constant such that for any $v \in V$ there exists a decomposition $v = \sum_{i=0}^{p} I_i v_i$, $v_i \in V_i$ with*

$$\sum_{i=0}^{p} (v_i, v_i)_i \leq C_0 a(v, v) ,$$

and let

$$C_1 = max_{1 \leq j \leq p} \sum_{i=1}^{p} \varepsilon_{ij}$$

where $\varepsilon_{ij} = 0$ if $T_i T_j = 0$, and 1 otherwise. Then the abstract additive Schwarz method admits the following estimate

$$\kappa(\sum_{i=0}^{p} T_i) \leq \omega C_0 (1 + C_1) . \tag{22}$$

Similar convergence estimates hold for the multiplicative Schwarz method in which we update the residual in between each application of the subspace correction operators T_i. Another attractive variant is the hybrid Schwarz preconditioner

$$\mathcal{P}(\cdot) = T_0 + (I - \sum_{i=1}^{p} T_i) T_0 , \tag{23}$$

for which it is known that $\kappa(\mathcal{P}) \leq \kappa(\sum_{i=0}^{p} T_i)$, [23]. We see that (23) can be viewed as a multiplicative Schwarz method on the splitting $V = V_0 + V_*$, $V_* = V$, where the bilinear form on V_* is approximated with an additive Schwarz splitting into V_1 to V_p. Also note that the multiplicative Schwarz method and the operator (23) can be symmetrized by including a sweep of the local subspace corrections (in opposite order) before and after the coarse subspace correction. This implies that we can use the preconditioned conjugate gradient algorithm to accelerate the DD iteration.

3.1 Convergence analysis

Let $\mathcal{N}_K$ be a set of coarse grid nodal points on Γ and let Ω be decomposed into the overlapping subdomains

$$\Omega_i = \cup\{K \in \mathcal{K}^H : \partial K \cap x_i \neq \emptyset, \ x_i \in \mathcal{N}_K\} ,$$

where we require $\Omega_i \cap \mathcal{N}_K = x_i$. Now, define $V_i^h = V^h(\Omega_i)$. The local Schwarz operators T_i are defined to be the orthogonal projection onto V_i^h with respect to $(\cdot, \cdot)_\Sigma^{1/2}$. Thus, we immediately obtain,

$$(T_i u, v)_\Sigma = (u, v)_\Sigma , \quad \forall u \in V^h , \ \forall v \in V_i^h .$$

We recall that $T_0 = (L^h)^T A_0^h L^h$. Hence, to obtain a proper Schwarz algorithm, we only need to define an appropriate bilinear form on V_0^h. To this end, we simply define the bilinear form $(\cdot, \cdot)_{\Sigma_0}$ on V_0^h such that,

$$(T_0 u, v)_{\Sigma_0} = (u, v)_\Sigma , \quad \forall u \in V^h , \ \forall v \in V_0^h . \tag{24}$$

To check that this bilinear form has the desired approximation property, we need to verify that the Schwarz parameter ω is bounded. Since T_0 maps V^h onto V_0^h, we may represent $v_0 \in V_0^h$ as $v_0 = T_0 v$ for some $v \in V^h$. Thus, by (12) and (24) we have

$$(v_0, v_0)_{\Sigma_0} = (v, v_0)_\Sigma = (T_0^{1/2} v, T_0^{1/2} v)_\Sigma$$
$$\lesssim a^h (L^h T_0^{1/2} v, L^h T_0^{1/2} v) .$$

But, since $L^h T_0^{1/2} = (A_0^h)^{1/2} L^h$, we have

$$a^h (L^h T_0^{1/2} v, L^h T_0^{1/2} v) = a^h ((A_0^h)^{1/2} L^h v, (A_0^h)^{1/2} L^h v)$$
$$= a^h (L^h v, A_0^h L^h v) .$$

Finally, since A_0^h is an orthogonal projection with respect to $a^h(\cdot, \cdot)^{1/2}$ and $A_0^h L^h v = L^h v_0$, we have

$$a^h (L^h v, A_0^h L^h v) = a^h (A_0^h L^h v, A_0^h L^h v)$$
$$= a^h (L^h v_0, L^h v_0)$$
$$\lesssim (v_0, v_0)_\Sigma ,$$

and it follows that $\omega \lesssim 1$. This confirms that the coarse subspace correction also fits into the Schwarz framework.

To obtain a bound on the condition number of our preconditioner we only need to bound the parameters C_0 and C_1 in (22). The parameter C_1 is bounded independent of the mesh parameters by a standard coloring argument, [23,24]. To bound C_0 we need to show that, for each $v \in V^h$, there exists a representation $v = \sum_{i=0}^{p} v_i$, $v_i \in V_i^h$, with

$$(v_0, v_0)_{\Sigma_0} + \sum_{i=1}^{p} (v_i, v_i)_\Sigma \leq C_0 (v, v)_\Sigma . \tag{25}$$

Owing to the equivalence relation (12), we may carry out the analysis in the equivalent finite element space $U^h = L^h V^h$. We thus define $U_i^h = L^h V_i$ and seek C_0 such that any $u \in U^h$ allows a decomposition $u = \sum_{i=0}^{p} u_i$, $u \in U_i^h$ with

$$\sum_{i=0}^{p} a^h (u_i, u_i) \leq C_0 a^h (u, u) . \tag{26}$$

We start by introducing the space of generalized discrete harmonic functions,

$$W_a^h(\mathcal{K}^H) = \{u \in U^h : a^h(u,v) = 0 \,, \; \forall v \in U_0^h(\mathcal{K}^H)\} \,,$$

where

$$U_0^h(\mathcal{K}^H) = \{u \in U^h : u = 0 \text{ at the nodal points on } \Gamma\} \,.$$

Now, let M^h be the space of nodal values on Γ and define the generalized discrete harmonic extension operator $H_a^h : M^h \to W_a^h$ by,

$$a^h(H_a^h \mu, u) = 0 \,, \; \forall u \in U_0^h(\mathcal{K}^H) \,. \tag{27}$$

It is important to observe that the space of generalized discrete harmonic functions can be viewed as the the space of functions with minimal energy with prescribed data on Γ. Indeed, if $\mu \in M^h$ and $u \in U^h$ is any function with $u|_\Gamma = \mu$, then, letting $v = H_a^h \mu$ and applying (27) twice, we obtain

$$0 \le a^h(u - v, u - v) = a^h(u, u - v)$$
$$= a^h(u, u) - a^h(v, v) \,.$$

Thus, $a^h(v, v) \le a^h(u, u)$ for all $u \in U^h$ with $u|_\Gamma = \mu$. We also need to define the following local discrete norm,

$$|u|_{a,h,K}^2 = \sum_{X \in \mathcal{X}^h(K)} \int_X \nabla u \cdot a(x) \nabla u \,.$$

We omit the subscript a and write $|\cdot|_{h,K}$, W^h and H^h if $a(x) \equiv I$. We are now ready to state our main result.

Theorem 2 *Assume there exist a constant $\beta > 0$ such that each $u \in U^h$ allows a decomposition $u = \sum_{i=0}^p u_i$, $u_0 \in H^h M_0$, $u_i \in U_i^h$, $1 \le i \le p$, with*

$$\sum_{i=0}^p |u_i|_{h,K}^2 \le \beta |u|_{h,K}^2 \,, \; \forall K \in \mathcal{K}^H \,. \tag{28}$$

Furthermore, let $\gamma_{1,K}$ and $\gamma_{2,K}$ be the sharpest positive constants such that for all $\mu \in M^h$ we have,

$$\gamma_{1,K} |H^h \mu|_{h,K}^2 \le |H_a^h \mu|_{a,h,K}^2 \le \gamma_{2,K} |H^h \mu|_{h,K}^2 \,. \tag{29}$$

Then, each $u \in U^h$ allows a decomposition $u = \sum_{i=0}^p u_i$, $u_i \in U_i^h$ with

$$\sum_{i=0}^p a^h(u_i, u_i) \le \beta \gamma \, a^h(u, u) \,. \tag{30}$$

where $\gamma = \max_{K \in \mathcal{K}^H} (\gamma_{2,K}/\gamma_{1,K})$.

Proof : First observe that any function $u \in U^h$ has a unique decomposition $u = w + u_*$, $w \in W_a^h$, $u_* \in U_0^h(\mathcal{K}^H)$ since W_a^h is, by definition, the orthogonal complement to $U_0^h(\mathcal{K}^H)$ with respect to $a^h(\cdot, \cdot)$. We thus have

$$a^h(u, u) = a^h(w, w) + a^h(u_*, u_*)$$
$$= a^h(w, w) + \sum_{K \in \mathcal{K}^H} a^h(u_{*,K}, u_{*,K}) \,.$$

But, since each $K \in \mathcal{K}^H$ is contained in at least one subdomain Ω_i, it is clear that we may represent $u_* = \sum_{i=1}^p u_{*,i}$, $u_{*,i} \in U_i^h \cap U_0^h(\mathcal{K}^H)$ with

$$a^h(u_*, u_*) = \sum_{i=1}^p a^h(u_{*,i}, u_{*,i}) \,.$$

Now if $\mu = u|_\Gamma$ and $w = H_a^h \mu$ allows a decomposition $w = \sum_{i=0}^p v_i$, $v_i \in U_i^h$, then we also have $w = \sum_{i=0}^p w_i$, $w_i = H_a^h(v_i|_\Gamma)$. Thus, letting $u_i = u_{*,i} + w_i$ with $u_{*,0} = 0$ we obtain

$$\sum_{i=0}^p a^h(u_i, u_i) = \sum_{i=0}^p a^h(u_{*,i}, u_{*,i}) + a^h(w_i, w_i)$$
$$= a^h(u_*, u_*) + \sum_{i=0}^p a^h(w_i, w_i) \,.$$

Hence, it only remains to bound the energy of the components w_i in terms of the energy of w. It follows from (28) that each $v \in W^h$ allows a decomposition $v = \sum_{i=0}^p v_i$, $v_0 \in H^h M_0$, $v_i \in U_i^h$, $1 \le i \le p$, with

$$\sum_{i=0}^p |v_i|_{h,K}^2 \le \beta |w|_{h,K}^2 \,, \; \forall K \in \mathcal{K}^H \,. \tag{31}$$

But, then we also have that $v = \sum_{i=0}^p w_i$ where $w_i = H^h(v_i|_\Gamma)$. Thus, by the minimal energy property of the generalized discrete harmonic functions we have that $|w_i|_{h,K} \le |v_i|_{h,K}$ and the desired result follows from (31).

Now, let $v = H^h \mu$ be decomposed as in (31) and define and $\mu_i = v_i|_\Gamma$. Then, by (29), we have

$$\sum_{i=0}^p |H_a^h \mu_i|_{a,h,K}^2 \le \sum_{i=0}^p \gamma_{2,K} |H^h \mu_i|_{h,K}^2$$
$$\le \beta \gamma_{2,K} |H^h \mu|_{h,K}^2$$
$$\le \beta \gamma |H_a^h \mu|_{a,h,K}^2 \,.$$

The desired result now follows by summing over $K \in \mathcal{K}^H$. This completes the proof of theorem 3.1.

A sufficient condition for (28) to hold is the existence of an operator $J : U^h \to H^h M_0$ such that for each $K \in \mathcal{K}^H$ and $u \in U^h$ we have

$$|Ju|_{h,K}^2 \lesssim \beta |u|_{h,K}^2 \,,$$
$$\|u - Ju\|_{L^2(K)}^2 \lesssim \beta H^2 |u|_{h,K}^2 \,.$$

Estimates of this kind is has been established for a great variety of coarse spaces in the finite element literature, see e.g. [8, 13, 22, 24]. For instance, if conforming linear finite elements are used on both the fine and coarse scale, then it was proved by Bramble and Xu, [8], that $\beta \lesssim \log(H/h)$ in 2D and $\beta \lesssim H/h$ in 3D. If non-conforming linear finite elements are applied on both scales, then β can be bounded independently of the mesh parameters, [22]. Note that this corresponds to non-matching boundary conditions so that $M_0 \not\subset M^h$.

If $a_\varepsilon(x)$ is a symmetric periodic matrix in $\mathcal{R}^{d \times d}$, then the homogenized matrix a_0 satisfy the convergence of energies, [18] section 1.3,

$$\lim_{\varepsilon \to 0} |H_{a_\varepsilon}^h \mu|_{a_\varepsilon, h, K}^2 = |H_{a_0}^h \mu|_{a_0, h, K}^2 \,, \quad \forall \mu \in M^h \,.$$

Moreover, by the Voigt-Reiss' inequality, [18], we have

$$\left(\frac{1}{K} \int_K a_\varepsilon^{-1}(x) \, dx\right)^{-1} \le a_0 \le \left(\frac{1}{K} \int_K a_\varepsilon(x) \, dx\right) \,,$$

where the inequalities are to be interpreted in a spectral sense. The upper and lower bounds for the homogenized

matrix are sharp in the sense that they are attained for perfectly stratified media with flow either perpendicular or parallel to the layers. But, they are also crude in the sense that they do not account for the heterogeneous structures within the periodic cells. Many other and better bounds can be found in the literature on upscaling for porous media flow, and some of these bounds can be found in [20].

Though $a(x)$ is not periodic in general, the multiscale analysis only concerns the local nature of $a(x)$ and we may think of K as a periodic cell in an infinite periodic media. We therefore expect similar bounds to hold so that

$$\frac{\gamma_{2,K}}{\gamma_{1,K}} \leq \frac{\kappa \left(\int_K a(x) \, dx \int_K a^{-1}(x) \, dx \right)}{|K|^2} \ .$$

Unfortunately, this factor can still be quite large, but we have not yet been able to see a strong dependence of this kind on the local heterogeneous structures in practice.

4 Implementational issues

The use of a multiscale method as a coarse solver for DD type algorithms should reduce the negative impact on the convergence rate caused by the subgrid heterogeneous structures provided that we select proper boundary conditions for the base functions. If we want to employ smooth boundary conditions, e.g., piecewise linear, then the coarse grid should preferably be chosen so that we "minimize" the presence of strong heterogeneous features that penetrate the grid-block interfaces. This might suggest the use of flexible gridding schemes like the non-uniform coarsening approach proposed by Durlofsky et al., [12]. The non-uniform coarsening technique, which generates grids that are finely gridded in high flow regions, was developed because it was acknowledged that it is important to model the high flow regions in porous media flow correctly in order to produce reliable production scenarios. If we use a fixed grid that does not reflect the heterogeneous formations, then we may have to use an oversampling strategy in order to obtain robust boundary conditions.

We shall for the most part employ the hybrid Schwarz preconditioner (23). One loop of the DD iteration thus consists of the following steps,

(i) $v_0^{k+1} = v^k + T_0(v^h - v^k),$
(ii) $v_i^{k+1} = T_i(v^h - v_0^{k+1}) , \ i = 1, \dots, p,$
(iii) $v^{k+1} = v_0^{k+1} + \sum_{i=1}^{p} \sum_{K \subset \Omega_i} n(K)^{-1} \chi_K v_i^{k+1},$

where v^k is the current approximation to v^h after k iterations and χ_K is the characteristic function with respect to K. The partition of unity $\nu(\Omega) = \{n(K)^{-1}\chi_K\}$ is needed to ensure convergence since the subdomains overlap, but it does not alter the Schwarz analysis, [4].

On a single processor computer, the subspace corrections are solved successively. This means that the subdomains Ω_i should be chosen so that the local subspace corrections can be solved efficiently with a simple iterative method such as the conjugate gradient method.

It may be appealing to view the distinct heterogeneous features in the permeability field as building blocks that can be used to define the subdomains. However, when we use a multiscale method as a coarse solver, then the main purpose of the subdomain solvers is to approximate the solution at the grid-block interfaces. It is therefore natural to use the coarse grid as a starting point when we design the local subdomains. For instance we may associate with each grid block K the subdomain

$$\Omega_K = \{x \in \Omega : dist(x, K) < \delta\} \qquad (32)$$

where δ is some specified overlap distance, see Figure 3.
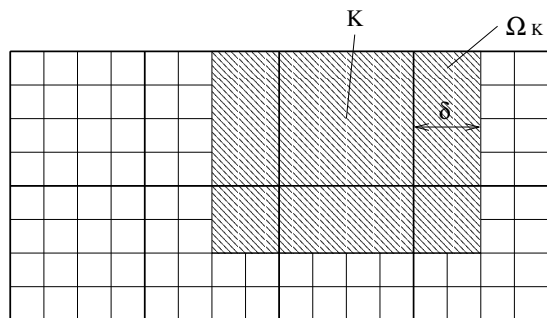
Fig. 3. Example of a selection of subdomains with a two row overlap

The multiscale base functions will only have support in a few neighboring grid blocks K and the number of base functions will typically be roughly the same as the number of grid blocks. This implies that the computation time associated with the construction of the multiscale base functions is comparable with one sweep of the local subspace corrections (ii). The construction of the multiscale base functions and the local subspace corrections in (ii) can be computed in parallel. Hence, if one has a multi-processor computer available, then one can distribute the work associated with the construction of the base functions and the local subspace corrections among the processors. Also, if we use a multiplicative Schwarz algorithm then we can use a coloring argument [23,24] to group the subdomains into a few subsets for which the subdomain subspace corrections can be computed independently.

5 Numerical Results

Our primary purpose in this section is to try to reveal how the convergence rate of the DD iteration depends on the heterogeneous structures. In particular, we try to reveal how the convergence rate parameter γ depends on the local heterogeneous structures, and how the convergence rate parameter β depends on the selection of boundary conditions for the multiscale base functions. For the latter case, it is of special interest to see if we can select boundary conditions for the multiscale base functions which allow β to be bounded independent of the ratio between the mesh parameters H/h.

Hence, let $\mathcal{T}^h$ and $\mathcal{K}^H$ be uniform partitionings of $\Omega = [0,1]^d$ into squares or cubes with edges of length h and H respectively. The right hand side in (1) is chosen to be $f \equiv 1$ and the stopping criteria is set to be when the relative size of the current residual to the initial residual in the L^2-norm drops below 10^{-5}, i.e. when $\|f - \Sigma^h v^k\|_{L^2(\Omega)} \leq 10^{-5} \cdot \|f\|_{L^2(\Omega)} = 10^{-5}$. Since the convergence rate parameter γ is independent of the macroscopic heterogeneous structures, we use periodic media to track down the relation between γ and the heterogeneous formations in Ω. Similarly, since β is independent of the local heterogeneous structures, we use quasi-homogeneous media to track down the relation between β and the heterogeneous formations in Ω.

5.1 Periodic Media

We study three different periodic structures. The first choice $k^h_{1,p}(x)$ resembles the coefficient function which brought out the large contrasts in [4] and contain a high permeability spike at the center of the coarse grid blocks, i.e. the periodic cells. The other two choices $k^h_{2,p}(x)$ and $k^h_{3,p}(x)$ are respectively a coefficient function with a high permeability streak and a coefficient function with a checkerboard kind of structure. To be more precise, let $Y = [0,H]^d$ and define $k^h_{1,p}$, $k^h_{2,p}$ and $k^h_{3,p}$ in Y as follows.

First define $\sigma_1(x) = (2/H)dist(x, \partial Y)$ and let $\sigma_2(x)$ be the Y-periodic function with a diagonal high permeability streak with $\sigma_2(x) = 2$ inside the streak and $\sigma_2(x) = 1$ outside the streak. In three dimensions we use the same pattern in the x-y plane, and have constant permeability in the z direction, i.e. $\sigma_2(x,y,z) = \sigma_2(x,y,0)$ for all $z \in [0,H]$. Finally, let $\sigma_3(x)$ be the 2×2 or $2 \times 2 \times 2$ checkerboard coefficient function in Y with values 1 and 2 in two dimensions and values, $1, 2, 3$ and 4 in three dimensions. We then define

$$k^h_{i,p}(x) = \sigma_i(x)^p \ , \ i = 1, 2, 3 \ .$$

The functions $\{k^h_{i,p}(x) : i = 1, 2, 3\}$ are plotted for $p = 8$ in Figure 4. We observe that the parameter p scales the local aspect ratios, and we should therefore be able to investigate if a scaling of the aspect ratios have an important effect on the convergence rate of the DD iteration.
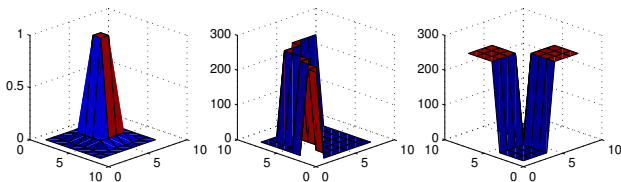

Fig. 4. Plots of $k^h_{1,p}$, $k^h_{2,p}$ and $k^h_{3,p}$ in $\mathcal{R}^2$ with $p = H/h = 8$.

5.1.1 Numerical results in 2D

We first select boundary conditions for the multiscale base functions so that the induced MsFEM is the "multiscale extension" of the bilinear FEM, i.e. the boundary conditions for the base functions are linear on each edge and determined by the requirement $\mu_i(x_j) = \delta_{ij}$ where x_j range over the set of vertices for the coarse grid blocks. We compare the induced MsDDM with the DDM obtained by replacing the "bilinear" MsFEM with the standard bilinear FEM. Figure 5 shows iterations counts for $h = H^2 = 1/64$ and $k^h_{1,p}$, $k^h_{2,p}$ and $k^h_{3,p}$ as a function of p.
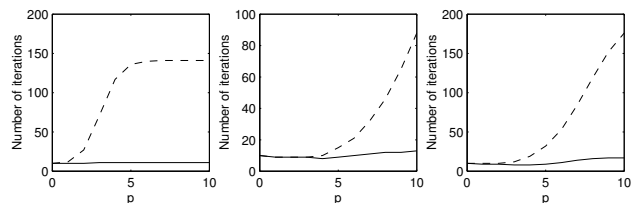

Fig. 5. Iteration counts for the DD algorithms with the standard bilinear FEM coarse solver (dashed line) and the "bilinear" MsFEM coarse solver (solid line) as a function of p. Left: $k^h_{1,p}$. Middle: $k^h_{2,p}$. Right: $k^h_{3,p}$.

We see that the iteration count for the "bilinear" MsDDM is stable and nearly independent of the local aspect ratios. In contrast, we see that the convergence rate for the DDM using standard bilinear finite elements deteriorate rapidly with p for each of the three coefficient functions. This clearly illustrates that coarse grid solvers constructed from (smooth) base functions that are not adaptive to the local heterogeneous structures can not be expected to perform well if the permeability distribution contain sharp contrasts at the subgrid level.

We now select boundary conditions for the multiscale base functions which correspond to the popular face based coarse solver in the literature on DD methods for elliptic partial differential equations. Thus, let E_{ij} be the edge common to the blocks K_i and K_j in $\mathcal{K}^H$ and define

$$\mu_{ij}(x) = \begin{cases} 1 \text{ if } x \in E_{ij} \ , \\ 0 \text{ otherwise .} \end{cases}$$

The multiscale base functions generated by the boundary conditions μ_{ij} then generate a coarse space which take constant values on each edge E_{ij}, but is in general discontinuous at the vertices of the coarse grid elements. We compare the induced MsDDM with the DDM obtained by replacing the face-based MsFEM with the standard face based coarse solver.

Figure 6 shows iteration counts for $h = H^2 = 1/64$ and $k^h_{1,p}$, $k^h_{2,p}$ and $k^h_{3,p}$ as a function of p. Again we see that the iteration count for the MsDDM is stable and nearly independent of the local aspect ratios. This convergence behavior is in sharp contrast to the performance of the DDM with the standard face based coarse grid solver which deteriorate rapidly with p for each of the three coefficient functions. The two MsDDM's discussed in this section therefore show the same ability to capture the essential subgrid information and indicate that γ is bounded independent of the local heterogeneous formations in $\mathcal{R}^2$.
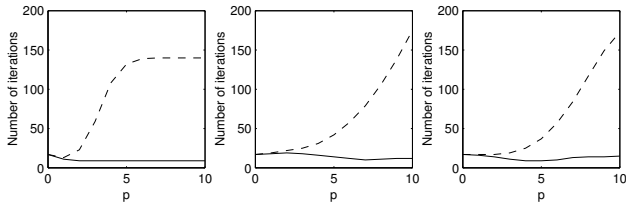
Fig. 6. Iteration counts for the DD algorithms with the standard face based coarse solver (dashed line) and the face based MsFEM coarse solver (solid line) as a function of p. Left: $k_{1,p}^h$. Middle: $k_{2,p}^h$. Right: $k_{3,p}^h$.

5.1.2 Numerical Results in 3D

Now, consider the MsDDM induced by the multiscale version of the trilinear FEM. The boundary conditions for the multiscale base functions are thus bilinear on each interface F and determined by the requirement $\mu_i(x_j) = \delta_{ij}$ where x_j ranges over the set of vertices for the coarse grid blocks. We compare the induced MsDDM with the DDM using the standard trilinear FEM as the coarse grid solver. Figure 7 shows iteration counts for $h = H^2 = 1/64$ and $k_{1,p}^h$, $k_{2,p}^h$ and $k_{3,p}^h$ as a function of p.
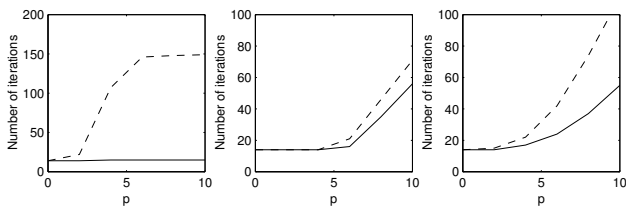
Fig. 7. Iteration counts for the DD algorithms with the standard trilinear FEM coarse solver (dashed line) and the "trilinear" MsFEM coarse solver (solid line) as a function of p. Left: $k_{1,p}^h$. Middle: $k_{2,p}^h$. Right: $k_{3,p}^h$.

Figure 7 shows that the convergence rate for the DDM induced by using the trilinear FEM as the coarse grid solver deteriorates quickly for each of the three coefficient functions, and that the number of iterations to reach convergence grows rapidly with p. We see that the iteration count for the "trilinear" MsDDM is stable for $k_{1,p}^h$, but, unfortunately the convergence rate now starts to deteriorate with p for $k_{2,p}^h$ and $k_{3,p}^h$. This indicates that the convergence rate is more sensitive to the selected boundary conditions in three spatial dimensions than in two spatial dimensions. The poor convergence property of the MsDDM for $k_{2,p}^h$ and $k_{3,p}^h$ is due to the fact that the bilinear boundary conditions that we use to define the multiscale base functions imply that the approximation space V_0 is smooth on the interface structure, while the elliptic solution is nearly discontinuous at the grid-block vertices.

One way to regain a stable convergence rate is to select boundary conditions that are adaptive to the heterogeneous structures at the coarse grid-block interfaces. This might, however, seem a bit cumbersome. Another

approach is therefore to select boundary conditions that impose less continuity constraints on the interface structure. We therefore select boundary conditions for the multiscale base functions that correspond to the 3D version of the face-based coarse solver. Thus, let F_{ij} be the interface between K_i and K_j in $\mathcal{K}^H$ and define

$$\mu_{ij}(x) = \begin{cases} 1 \text{ if } x \in F_{ij} \ , \\ 0 \text{ otherwise} \ . \end{cases} \tag{33}$$

These boundary conditions allow functions in V_0 to be discontinuous at the grid block vertices, but not on the interfaces. We compare the face-based MsDDM with the DDM induced by the traditional face based coarse solver. Figure 8 shows iteration counts for $h = H^2 = 1/64$ and $k_{1,p}^h$, $k_{2,p}^h$ and $k_{3,p}^h$ as a function of p.
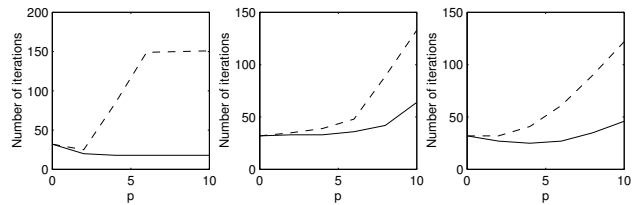
Fig. 8. Iteration counts for the DD algorithms with the standard face based coarse solver (dashed line) and the face based MsFEM coarse solver (solid line) as a function of p. Left: $k_{1,p}^h$. Middle: $k_{2,p}^h$. Right: $k_{3,p}^h$.

The DDM induced by the face based coarse solver show poor convergence properties for these heterogeneous structures and displays a similar convergence behavior to the DDM induced by the trilinear FEM coarse solver. The MsDDM again display a stable convergence rate for $k_{1,p}^h$, and the convergence rate is more stable for $k_{2,p}^h$ and $k_{3,p}^h$ than we observed for the "trilinear" MsDDM. However, as long as we do not attempt to resolve the heterogeneous features that penetrate the interface structure, then we must expect to see some dependence on the local heterogeneous structures. But there is no doubt that the two MsDDM's that we have studied here perform superior to the associated DDM's that do not employ a MsFEM as a coarse solver. As such they offer the possibility of significant savings in computation time over traditional domain decomposition methods. Whether they will prove to be competitive with other state-of-the-art preconditioning techniques, like multigrid methods, is a topic for further research.

5.2 Quasi-Homogeneous Media

We now investigate how the selection of boundary conditions for the multiscale base functions influence the convergence rate. In particular, we want to study how the parameter β in (28) depends on the heterogeneous formations in Ω. Since β is independent of the local heterogeneous structures, we apply the MsDDM's to problems with quasi-homogeneous coefficients, i.e. problems

where the permeability $a(x)$ is constant within the coarse grid elements. Thus, for each K let $\sigma^H(K)$ be sampled at random from $(0,1)$ and define

$$k_p^H(x) = \sigma^H(x)^p \ .$$

We see that the parameter p magnifies the discontinuities across the coarse grid interfaces. We should therefore be able to reveal if the convergence rate of the proposed Ms-DDM's depend on the quasi-homogeneous coefficients. We also observe that the convergence rate parameter γ is identical to one, so that the convergence rate should only depend on β.

For the quasi-homogeneous coefficient problem, the MsDDM's discussed above reduce to the associated traditional coarse grid solvers. The bilinear or trilinear FEM coarse grid solvers and the two face based coarse grid solvers inherit different approximation properties. The bilinear and trilinear FEM coarse grid solvers work well for smooth coefficient problems, but not so good for discontinuous coefficient problems because they are not able to handle the singularities at the vertices of the elements properly. The face based coarse grid solvers, on the other hand, allow the solution to be discontinuous at the vertices and handle discontinuities much better, but does not work so well for smooth coefficient problems. This suggests that it might be a good idea to construct a coarse grid solver using both bilinear or trilinear and face-based base functions. After all, it is worthwhile to spend extra effort on constructing the coarse subspace correction if it can reduce the number of iterations, and thereby reduce the total computational cost.

We first study the DDM for the 2D case where the coarse solvers are constructed with bilinear, face-based and both bilinear and face-based base functions respectively. Figure 9 illustrates that the bilinear FEM works well for smooth coefficient problems, but that the convergence rate deteriorates with p. The face-based coarse solver, on the other hand, shows good performance for highly discontinuous coefficients, but not so good for the homogeneous coefficient problem with $p = 0$. Combining the two generates a coarse solver which seem to be nearly independent of both p and the mesh parameter ratio H/h, and hence, in particular, allows β to be almost independent of p and the problem dimensions.

Further testing showed that if the bilinear FEM and face based base functions were replaced with their multiscale variants, then the convergence behavior depicted above was not affected by adding heterogeneous structures to the coarse grid blocks. This confirms that we can decompose the convergence rate as the product of γ and β. We have therefore shown how one can construct a nearly optimal DD preconditioner for the elliptic problem (1)-(2) in $\mathcal{R}^2$ which seems to converge at a rate independent of the elliptic coefficients.

Finally we turn to the case with a quasi-homogeneous media in 3D. Figure 10 shows iteration counts using the DDM's induced by the coarse solvers constructed with trilinear, face-based and both trilinear and face-based base functions respectively. We see much the same situation as in two dimensions. In particular, by using both
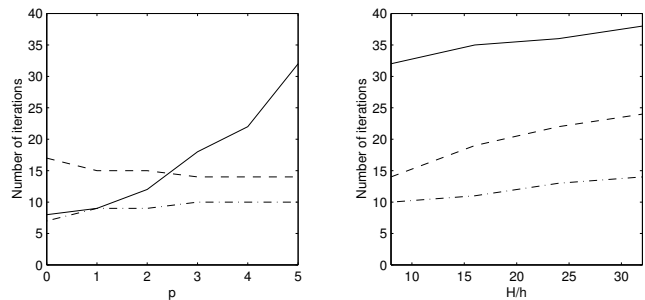
Fig. 9. Iteration counts for the DDM's induced by bilinear (solid line), face-based (dashed line) and bilinear + face-based (dash-dot line) base functions for the coarse subspace correction. Left: Iteration counts for $h = H^2 = 1/64$ as a function of p. Right: Iteration counts for $p = 5$ and $H = 1/8$ as a function of H/h.

trilinear and face based base functions we achieve an iteration count which indicates that β is nearly independent of p and the problem dimensions.

Since we recall that the numerical tests in section 4.1.2 showed that γ was not independent of the local heterogeneous structures, we can not hope to achieve a (nearly) optimal DD preconditioner for the elliptic problem (1)-(2) in three dimensions by replacing the trilinear FEM and face based base functions with their multiscale variants. However, further tests showed that by adding heterogeneous structures to the coarse grid blocks, we obtain a rate of convergence which is consistent with the convergence rate that we observed for periodic media. Thus, the splitting of the condition number estimate for the DD preconditioner in (30) into a parameter γ which depends on the local heterogeneous structures and a parameter β which depend on the global structures seem to be justified.
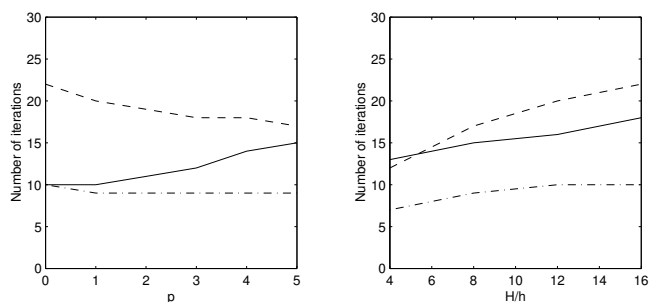
Fig. 10. Iteration counts for the DDM's induced by trilinear (solid line), face-based (dashed line) and trilinear + face-based (dash-dot line) base functions for the coarse subspace correction. Left: Iteration counts for $h = H/8 = 1/32$ as a function of p. Right: Iteration counts for $p = 5$ and $H = 1/4$ as a function of H/h.

5.3 A test case with real reservoir data

We conclude this study by showing that the MsDDM induced by the face-based coarse solver performs well for a test-case with real data taken from the the 10th SPE comparative solution project, model 2, see [9]. A schematic of the reservoir domain is shown in Figure 11. In order not to deviate from the framework that we have developed in the previous sections we impose homogeneous Dirichlet boundary conditions on the boundary of the reservoir domain instead of no-flow boundary conditions as was used in [9]. However, Neumann boundary conditions can be handled with no extra difficulty.
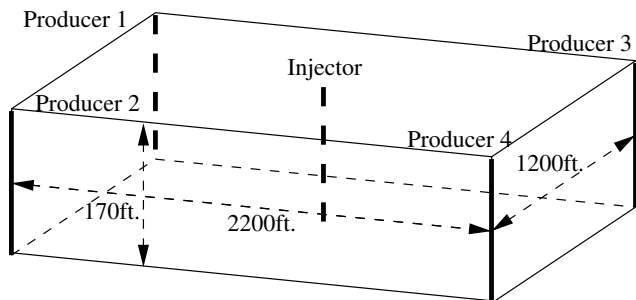
Fig. 11. The figure depicts the reservoir domain with a producer at each corner and an injector at the center.

The permeability field consists of two separate heterogeneous formations that are sampled from the SPE comparative solution project, model 2, [9]. The top 70 ft. represent the Tarbert formation and the bottom 100 ft. represent the Upper Ness formation. We have plotted the logarithm of the average of the permeability layers in the Tarbert and Upper Ness formations in Figure 12.
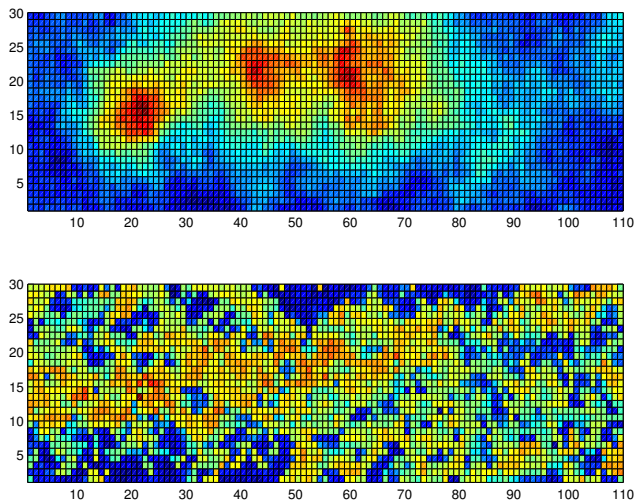
Fig. 12. The figure illustrates the heterogeneous structures in the Tarbert formation (top) and the Upper Ness formation (bottom) that was used in the 10th SPE comparative solution project, model 2.

Though the ratio of the extreme permeability values is "almost" the same for the two heterogeneous formations (∼ 8 versus ∼ 12 orders of magnitude), the permeability field for the the Tarbert formation is much smoother than the permeability field for the Upper Ness formation. In fact, the contrasts in the permeability field for the Upper Ness formation are so strong that simple iterative methods will not converge unless the discretized linear system has been preconditioned with some robust preconditioner.

The purpose of this section is not to compare the proposed MsDDM's with traditional DDM's. Instead we want to show that even though the convergence rate for the MsDDM's may deteriorate in the presence of strong heterogeneous structures like we have in the Upper Ness formation if we use simple smooth boundary conditions, we may still achieve good convergence behavior by using the preconditioned conjugate gradient (PCG) method. We therefore apply the MsDDM's to the elliptic problems that arise from the two heterogeneous formations separately, instead of having the Tarbert formation on top of the Upper Ness formation.

Hence, let the boundary conditions for the multiscale base functions be defined by (33) and let the subdomains be defined by (32) using a two row overlap. For problems with such an extreme range of scales it is necessary to use the Multiplicative Schwarz method to ensure convergence. Thus, denote by MsDD-MS the Multiplicative Schwarz method and by MsDD-PCG the PCG algorithm induced by the symmetrized Multiplicative Schwarz method. A description of the PCG method can be found in any text book on iterative methods for sparse linear systems such as [Saad], but we have also included it in the appendix for completeness.

The fine grid for the Tarbert formation and Upper Ness formation that we employ here consists of $60 \times 110 \times 35$ and $60 \times 110 \times 50$ cells respectively. For both cases the coarse grid is chosen so that each grid block consists of $10 \times 10 \times 5$ grid cells. Iteration counts, i.e. the number of sweeps of the respective DD methods that is needed to reach convergence, is shown in Table 1.

Algorithm	Tarbert form.	Upper Ness form.
MsDD-MS	37	> 500
MsDD-PCG	11	24

Table 1. The table shows iteration counts for the MsDD-MS and MsDD-PCG algorithms for when applied to (1),(2) with data sampled from a Tarbert formation and a very heterogeneous Upper-Ness formation.

We see that the MsDD-MS method performs reasonably well for the Tarbert formation, but for the problem with data from the Upper Ness formation the convergence rate starts to stagnate and the MsDD-MS method needs an excessive number of iterations to converge. The situation does not improve much if we replace the MsDD-MS with the symmetrized version of the Multiplicative Schwarz method. Indeed, it is primarily the coarse grid

solver that governs the convergence rate, although it helps to extend the overlap regions for the subdomains defined by (32). We should also be able to reduce the number of iterations by selecting better boundary conditions for the base functions, but we see that the MsDD-PCG algorithm performs well even if we do not extend the overlap region or alter the boundary conditions for the base functions. This shows that it is possible to achieve a very robust and efficient solver for elliptic problems with multiple scales by using a DD method with small subdomain overlap and a relatively simple multiscale coarse grid solver.

6 Concluding Remarks

We have demonstrated that the proposed domain decomposition methods can be used to solve the elliptic problem arising from flows in strongly heterogeneous porous media with a permeability distribution that may span over multiple length scales. The numerical tests indicate that the multiscale domain decomposition methods converge at a rate independent of the heterogeneous features at the subgrid level in $\mathcal{R}^2$, but they reveal that we may see a weak growth in the convergence rate in $\mathcal{R}^3$ if we do not use boundary conditions that are adaptive to the heterogeneous structures at the grid-block interfaces.

All the multiscale domain decomposition methods considered in this paper lead to a significant gain in iterations compared with their respective non-multiscale variants. These non-multiscale variants employ coarse solvers which are among the most popular coarse solvers in the domain decomposition literature. We have illustrated that each of them induce a convergence rate which may deteriorate rapidly as the local aspect ratios blow up. The multiscale domain decomposition methods can therefore give substantial computational savings over the traditional domain decomposition methods. As the elliptic coefficients arising from heterogeneous porous formations can vary several orders of magnitude at the microscale level, we conclude that the multiscale domain decomposition methods can be a very effective tool for simulating porous media flows.

Since we are dealing with a transport phenomena, we have developed a finite volume version of the MsFEM, and constructed a corresponding domain decomposition preconditioner. The convergence analysis for this preconditioner rests on the assumption that the subgrid discretization is mathematically equivalent with an appropriate non-conforming FEM on a dual grid. That is, we assume the two discretization matrices give rise to equivalent norms under the correspondence induced by a linear map between the two approximation spaces. The virtue of this equivalence relation was established for the two-point flux-approximation finite volume scheme on a-orthogonal grids and for the multi-point flux approximation finite volume scheme, the O-method, on general quadrilateral grids in two dimensions. It was further indicated that it extends to general polygonal and polyhedral grids by considering similar dual grids.

We would like to emphasize that we have not claimed that the proposed domain decomposition methods provide the only efficient solution strategy for elliptic problems with multiple scale coefficients. Indeed, multigrid methods are somewhat less sensitive to rapidly oscillatory coefficients, but their convergence properties do depend on the condition number of the discrete matrix. What we do claim, and have made an effort to show, is that the convergence rate of domain decomposition methods may deteriorate dramatically if we do not use a coarse solver which reflects the fine scale structures in the elliptic coefficients. The reason that we have not supplied computation times is that the DD iterations are run on a slow single processor computer using Matlab. The computation times are therefore not representative of the computation time that we can obtain with modern computers using e.g. C++ programming code.

The proposed domain decomposition methods have many important applications, but are perhaps particularly valuable for multi-phase flow simulations in heterogeneous porous media since these problems involve solving the elliptic part repeatedly throughout the simulation run. The computational cost associated with updating the pressure usually dominates the total computational cost, and an efficient preconditioner for the elliptic part is mandatory. The proposed domain decomposition methods are also naturally suited for parallel computing environments. They can therefore provide a valid alternative to upscaling for reservoir simulation, i.e. an alternative to upscaling the elliptic coefficients in order to run simulations on a coarsened grid. This possibility, and the use of more advanced boundary conditions for the multiscale base functions will be investigated in further work.

References

1. I. Aavatsmark, T. Barkve, Ø. Bøe, T. Mannseth, *Discretization on Unstructured Grids for Inhomogeneous, Anisotropic Media. Part I: Derivation of the Methods*, Siam J. Sci. Comp., 1998, 19(5): 1700-1716.

2. I. Aavatsmark, T. Barkve, Ø. Bøe, T. Mannseth, *Discretization on Unstructured Grids for Inhomogeneous, Anisotropic Media. Part II: Discussion and Numerical Results*, Siam J. Sci. Comp., 1998, 19(5): 1717-1736.

3. I. Aavatsmark, T. Barkve, Ø. Bøe, T. Mannseth, *Discretization on Non-Orthogonal, Quadrilateral Grids for Inhomogeneous, Anisotropic Media*, J. Comp. Physics, 1996, 127: 2-14.

4. J. Aarnes, T.Y. Hou, *Multiscale Domain Decomposition Methods for Elliptic Problems with High Aspect Ratios*, Acta Math. Appl., 2002, 18(1): 63-76.

5. D.N. Arnold, F. Brezzi, *Mixed and nonconforming finite element methods: implementation, postprocessing and error estimates*, Math. Model. and Numer. Anal., 1985, 19: 7-32.

6. I. Babuška, G. Caloz, E. Osborn, *Special Finite Element Methods for a Class of Second Order Elliptic Problems with Rough Coefficients*, SIAM J. Numer. Anal., 1994, 31: 945-981.

7. I. Babuška, E. Osborn, *Generalized Finite Element methods: Their Performance and their Relationship to Mixed Methods*, SIAM J. Numer. Anal., 1983, 20: 510-536.

8. J.H. Bramble, J. Xu, *Some Estimates For a Weighted L^2-Projection*, Math. Comp., 1991, 57(195): 463-476.

9. M.A. Christie, M.J. Blunt, *Tenth SPE comparative solution project: A comparison of upscaling techniques*, SPE 72469, 2001. Website: www.spe.org/csp

10. Z. Chen, *Equivalence Between Multigrid Algorithms for Non-Conforming and Mixed Methods for Second Order Elliptic Problems*, East-West J. Numer. Math., 1996, 4(1): 1-34.

11. Z. Chen, T.Y. Hou, *A Mixed Finite Element Method For Elliptic Problems With Oscillating Coefficients*, Math Comp., 2000.

12. L.J. Durlofsky, R.C. Jones, W.J. Milliken, *A nonuniform coarsening approach for the scale-up displacement processes in heterogeneous porous media*, Adv. Water Res., 1997, 20(5-6): 335-347.

13. M. Dryja, B.F. Smith, O.B. Widlund, *Schwarz Analysis of Iterative Substructuring Algorithms for Elliptic Problems in Three Dimensions*, SIAM J. Numer. Anal., 1994, 31(6): 1662-1694.

14. T.M. Hegre, V. Dalen, A. Henriquez, *Generalized Transmissibilities for Distorted Grids in Reservoir Simulation*, SPE 15622, Proc. SPE 61st Annual Technical Conference and Exhibition, New Orleans, 1986.

15. C. Hirsch, *Numerical Computation of Internal and External Flows. Vol. I*, John Wiley and Sons, New York, 1988.

16. T.Y. Hou, X-H Wu, *A Multiscale Finite Element Method for Elliptic Problems in Composite Materials and Porous Media*, J. Comput. Phys., 1997, 134(1): 169-189.

17. T.Y. Hou, X-H Wu, Z. Cai, *Convergence of a Multiscale Finite Element Method for Elliptic Problems with Rapidly Oscillating Coefficients*, Math. Comp., 1999, 68(227): 913-943.

18. V.V. Jikov, S.M. Kozlov, O.A. Oleinik, *Homogenization of Differential Operators and Integral Functionals*, Springer-Verlag, New York, 1994.

19. A. Quarteroni, A. Valli, *Domain Decomposition Methods for Partial Differential Equations*, Oxford University Press, Oxford, 1999.

20. P. Renard and G. de Marsily, *Calculating Equivalent Permeability*, Adv. Water Res., 1997, 20: 253-278.

21. Y. Saad, *Iterative methods for sparse linear systems*, PWS Publishing Co., Boston, 1996.

22. M. Sarkis, *Nonstandard Coarse Spaces and Schwarz Methods for elliptic problems with oscillating coefficients using non-conforming elements*, Numer. Math., 1997, 77: 383-406.

23. B.F. Smith, P. Bjørstad, W. Gropp, *Domain Decomposition Methods for Partial Differential Equations*, Cambridge University Press, Cambridge, 1996.

24. J. Xu, J. Zou, *Some Nonoverlapping Domain Decomposition Methods*, SIAM Rev., 1998, 40(4): 857-914.

Appendix

The preconditioned conjugate gradient method

Let A be a symmetric and positive definite matrix and consider the linear system

$$Ax = b. \tag{34}$$

Moreover, let M be a symmetric and positive definite preconditioner for A. Then the M-preconditioned conjugate gradient algorithm for (34) reads as follows:

(i) Pick an initial guess x_0

(ii) Set $r_0 = b - Ax_0$, $z_0 = M^{-1}r_0$ and $p_0 = z_0$.

(iii) For $j = 0, 1, \ldots,$ *until convergence*, do
    (a) $v_j = Ap_j$
    (b) $\alpha = (r_j, z_j)/(p_j, v_j)$
    (c) $x_{j+1} = x_j + \alpha p_j$
    (d) $r_{j+1} = r_j - \alpha v_j$
    (e) $z_{j+1} = M^{-1}r_{j+1}$
    (f) $\beta = (r_{j+1}, z_{j+1})/(r_j, z_j)$
    (g) $p_{j+1} = z_{j+1} + \beta p_j$.

(iv) Enddo.

Here $(\cdot, \cdot)$ is the Euclidean inner product. It is important to note that we do not have to compute M^{-1} explicitly, only its action is needed. Hence, M^{-1} may for instance be one multigrid cycle or a sweep of a loop of a domain decomposition iteration provided that the methods induce a symmetric and elliptic operator.